CHEMISTRY JOURNAL OF MOLDOVA. General, Industrial and Ecological Chemistry. 2024, 19(2), 83-92
ISSN (p) 1857-1727 ISSN (e) 2345-1688
http://cjm.ichem.md
https://doi.org/10.19261/cjm.2024.1220

SYNTHESIS, CHARACTERIZATION, HIRSHFELD AND ADMET ESTIMATION STUDIES OF NOVEL 3-(2,4,6-TRIMETHYL-PHENYLAMINO)-BUT-2-ENOATE

Mohamed Loughzail [a], Koffi Senam Etsè [b], Zaragoza Verez Guillermo [c], Rachid Touzani [d], Anna Moliterni [e], Abdessamad Tounsi [f], Mohamed Anouar Harrad [f,g*]

[a]*Molecular Chemistry Laboratory, Cadi Ayyad University, Marrakech 40000, Morocco*
[b]*Medicinal Chemistry Laboratory, Center for Interdisciplinary Research on Medicines (CIRM), University of Liège, B36 Av. Hippocrate 15 B-4000 Liege, Belgium*
[c]*X-Ray Diffraction Unit, RIAIDT, University of Santiago de Compostela, Campus VIDA, 15782 Santiago de Compostela, Spain*
[d]*Applied Chemistry and Environment Laboratory, University of Mohamed 1, Oujda, Morocco.*
[e]*Institute of Crystallography Via Amendola, 122/O, Bari 70126, Italy*
[f]*Environmental, Ecological, and Agro-Industrial Engineering Laboratory, Sultan Moulay Slimane University, Beni-mellal 23000, Morocco*
[g]*Regional center for Education training and formation, CRMEF 40000 Marrakech-Safi, Morocco*
[*]*e-mail: ma.harrad@yahoo.fr*

Abstract. The title compound 3-(2,4,6-timethyl-phenylamino)-but-2-enoate was obtained by condensation reaction of ethyl acetoacetate and 2,4,6-trimethyl-phenylamine. X-ray structural analysis identified the structure of the synthetized *β*-enaminoester, NMR spectroscopy complemented it, and the structure stabilized by intramolecular interactions. The intermolecular contacts were further analysed by the mapping of contacts descriptors d_{norm}, d_e, d_i, the shape-by-Shape index and surface property by electrostatic potential mapped on the Hirshfeld surface (HS). Data from density functional theory (DFT) was compared to experimental results for this process. Global reactivity factors such electronegativity, chemical hardness, potential, and softness were calculated using DFT. The effects of the molecular environment were accessed by analysing the electrostatic potentials surface mapped over the HS and the 3D-topology of energy frameworks. As a potential bioactive molecule, the physicochemical and ADME-Tox predictions were performed suggesting that compound **3** could be considered as promising drug candidate.

Keywords: *β*-enaminoester; X-ray diffraction, monoclinic space, Hirshfeld surface, ADMET-Tox.

Received: 20 August 2024/ Revised final: 2 December 2024/ Accepted: 5 December 2024

Introduction

β-Enaminoesters play a crucial role as a foundational component in the synthesis of various compounds with pharmacological attributes, encompassing antitumor antitubercular [1], antinociceptive [2], anticonvulsants [3], antibiotics [4], antifungal [5], anti-inflammatory [6], and antitumor [7]. Several reported heterocycles utilize *β*-enaminoesters as precursors in the synthetic pathways for pharmacologically active compounds, including pyrazoles, pyridinones, dibenzodiazepines, quinolines, oxazoles, and tetrahydrobenzoxazines [3,8,9]. Enaminoesters containing analogues have therefore proved effective in a wide range of drug classes.

Various synthetic approaches have been employed in the production of *β*-enaminoesters. Recent studies have explored new synthetic strategies such as electrochemical organic synthesis [10], and green chemistry protocol using onion extract [11]. Diverse catalysts, including $Ca(CF_3COO)_2$ [12], melamine-formaldehyde resin supported H^+ (MFRH) [13], $AlPO_4$ [14], Moroccan rock phosphate [15], silica-supported $Fe(HSO_4)_3$ under solvent-free conditions [16], silver nanoparticles [17], and bimetallic Ag–Cu alloy nanoparticles [18], bismuth(III) trifluoroacetate [19], molecular iodine [20], Amberlyst-15® [21], zeolite (ZSM-5) [22], $CoCl_2 \cdot 6H_2O$ [23], $ZnAl_2O_4$@ZnO [24], and ferric(III) ammonium nitrate [25] have been used to prepare the enaminone derivatives. The previous approach employed by Madje, B.R. *et al.* using direct synthesis involves the generation of

the *β*-dicarbonyl synthon through the reaction of an amine to produce the *β*-enaminoester in the presence of APTS under reflux conditions [25]. In this context, *β*-enaminoester, produced by direct condensation of a *β*-dicarbonyl with an amine *via* C–H insertion, could be considered as important precursors for the synthesis of *β*-enaminoesters since the N–H addition reaction could easily be carried out with amines under appropriate reaction conditions.

This paper presents the synthesis and characterization of a new *β*-enaminoester namely 3-(2,4,6-trimethyl-phenylamino)-but-2-enoate prepared by condensation reaction of ethyl acetoacetate and 2,4,6-trimethyl-phenylamine, in the presence of $CoCl_2$. X-ray structural analysis identified the structure of the synthetized *β*-enaminoester, NMR spectroscopy complemented it, and the structure stabilized by intramolecular interactions. Density functional theory (DFT) was used to obtain data for this reaction and was then compared with experimental results. DFT calculations were also used to determine global reactivity parameters, including electronegativity, chemical hardness, chemical potential and chemical softness. The results are expected to be useful for future *β*-enaminoester structure analyses and will also evaluate the physicochemical properties and ADME-Tox predictions of the potential bioactive molecule.

Experimental

Materials

Analytical grade chemicals including $CoCl_2{\cdot}6H_2O$, ethyl acetoacetate, and 2,4,6-trimethylamine were purchased from Janssen Chemica, and Sigma-Aldrich.

Instruments

The *^1H and ^{13}C NMR spectra* were recorded on a Bruker Avance 300 spectrometer at 300 MHz and 75 MHz, respectively, in $CDCl_3$ solvent.

Fourier-transform infrared (FTIR) *spectra* were obtained utilizing a Nicolet is 5 Thermo scientific spectrometer. Pellets were composed of 100 mg of finely powdered KBr and 2 mg of the sample.

Melting points were determined on *Banc Kofler apparatus*.

Synthesis of the β-enaminoeter: 3-(2,4,6-trimethyl-phenylamino)-but-2-enoate (3)

To a magnetically stirred mixture of the ethyl acetoacetate (5 mmol) and 2,4,6-trimethyl-phenylamine (5 mmol), $CoCl_2{\cdot}6H_2O$ (0.25 mmol) was added and the reaction mixture was stirred at room temperature for 20 minutes. At the end of the reaction, 10 mL of distilled water was added to the residue and extracted with diethyl ether (3×25 mL). The organic layer was dried over Na_2SO_4. The solvent was removed under reduced pressure. Pure *β*-enaminoester was obtained by column chromatography over silica gel using hexane/ethyl acetate as eluent. The pure product obtained as shiny colourless powder with a yield of 75%. m.p. 64–66°C. ^{1}H NMR *δ*/ppm: 1.13 (t, *J*= 6.6 Hz, 3H), 1.16–1.22 (m, 6H), 3.07–3.17 (m, 3H), 3.98 (d, *J*= 6.6 Hz, 2H), 4.53 (s, 1H), 7.01-7.15 (m, 2H, Ar), 9.73 (br s, 1H, NH). ^{13}C NMR *δ*/ppm: 14.70, 19.52, 22.64, 24.73, 28.34, 58.13, 83.76, 123.35, 128.05, 134.08, 146.91, 160.81, 170.31. IR (KBr) *υ* (cm^{-1}): 3255 (N–H), 2931, 999, 689, (Ph), 1640, 1255 (COOEt), 1569 (C=C–N).

Single-crystal X-ray diffraction analysis

Crystallographic data for compound **3** or the crystal structure determination, the previously reported procedure was used [26]. Briefly, the data were collected by applying the omega and phi scans method on a Bruker D8 Venture PHOTON III-14 diffractometer using INCOATEC multilayer mirror monochromated with MoK*α* radiation (*λ*= 0.71073 Å) from a microfocus sealed tube source at 100 K. Computing data and reduction were made with the APEX3 [27]. The structure was solved using SHELXT [28] and finally refined by full-matrix least-squares based on F^2 by SHELXL [29]. An empirical absorption correction was applied using the SADABS program. Software used to molecular graphics: ORTEP for Windows [30]. Software used to prepare material for publication: WinGX publication routines [30] and Mercury [31]. Crystal data, data collection and structure refinement details are summarized in Table 1. All non-hydrogen atoms were refined anisotropically and the hydrogen atom positions were included in the model on the basis of Fourier difference electron density maps. All CH and aromatic CH hydrogen (C–H= 0.95 Å) atoms were refined using a riding model with Uiso(H)= 1.2 Ueq(C). The methyl hydrogen (C–H= 0.98 Å) atoms were refined as a rigid group with torsional freedom [Uiso(H)= 1.5 Ueq(C)]. The H atoms positions and isotopic atomic factors of amine groups were refined as a free atom. Finally, Crystallographic data for **3** have been deposited at the Cambridge Crystallographic Data centre with the number CCDC-2323332. These data can be obtained free of charge from The Cambridge Crystallographic Data Centre *via* www.ccdc.cam.ac.uk/structures. The crystallographic data and details of the structure refinement are shown in Table S1.

Hirshfeld surface analysis

Molecular Hirshfeld surfaces [32-34], in the crystal structure were generated based CE-B3LYP, calculated as the sum of spherical atom electron densities [35,36]. These surfaces, which incorporate properties such as d_e, d_{norm}, shape-index, and 2D fingerprint plots, were created using CrystalExplorer 17.5 [37]. The (d_i) represents the distance to the nearest nucleus external to the surface, (d_e) denotes the distance to the nearest nucleus internal to the surface, and (d_{norm}) indicates the normalized contact distance. These calculations were utilized to pinpoint regions of intermolecular interactions on the Hirshfeld surfaces (HS) [38]. The surfaces were computed at a high resolution, with three-dimensional (d_{norm}) surfaces mapped using a colour scale ranging from −0.1670 Å (red) to 1.4062 Å (blue).

Results and discussion

The *β*-enaminoester was synthesized by condensation reaction of an amine with a dicarbonyl in the presence of $CoCl_2$ as a catalyst according to Scheme 1. The reaction was carried out solvent-free at room temperature with good yield. The obtained red crystalline compound is stable in air and soluble in organic solvents. The compound obtained underwent analysis using NMR, FTIR, and single crystal X-ray diffraction techniques.

Synthesis and NMR analysis

The synthesis of the title compound was carried out in accordance with the experimental procedures outlined in Scheme 1. Briefly, a stoichiometric quantity ethyl acetoacetate and 2,4,6-trimethyl-phenylamine are mixed in presence of $CoCl_2{\cdot}6H_2O$ at room temperature. The reaction completion was followed by TLC. At the end of the reaction followed by workup steps and purification by column chromatography, the desire product was isolated as colourless powder with a yield of 75%.

To ensure the identity of the obtained product, characterization using NMR analyses were performed (Figures S1 and S2 in supplementary information). The ^{1}H NMR spectrum highlights one singlet, at 9.56 ppm that could be easily attributed to the enamine N–*H* hydrogen atom [24]. The two aromatic protons are equivalent and appear as a singlet in the spectrum at 6.78 ppm. The *ortho* and *para* C*H*$_3$ of the mesityl proton are attributed to the singlets obtained at 2.07 and 2.16 ppm integrating for 6 and 3 protons respectively. For the enamine substituent, the ethylenic proton of the –C=C*H* group is identified as a singlet observed at 4.58 ppm. To confirm the presence of the ester group in the prepared compound, a ^{13}C NMR spectrum (Figure S2) of the title compound was recorded in $CDCl_3$ at 298 K to complete the nuclear magnetic resonance characterization. The chemical shifts of the carbon atom in the prepared compound are observed between 13.57 and 169.64 ppm. The O=*C*– carbon of the ester group appears at 169.64 ppm when the −*C*−O carbon is observed at 160.61 ppm. Finally, the *C*H$_3$ and *C*H$_2$ carbon of the ethyl group appear between 13.57 and 19.48 ppm.

After the NMR characterization, the IR spectrum of compound **3** was recorded (Figure S3). A wide, low-intensity band near 3255 cm^{-1} is associated with the N–H vibration. The different C-H vibrations are noted in various regions, with a band detected at 2931, 999, and 689 cm^{-1}. There is a strong band at 1616 cm^{-1} assignable to C=O stretching vibration. In addition, the in-plane deformation vibrations of C=O that is expected in the region 625±70 cm^{-1} is obtained at 748 cm^{-1} in IR. The streaking corresponding to N–C=C bond is observed at 1569 cm^{-1} [39].

X-ray crystal structure

An attempt was made to obtain single crystals suitable for X-ray diffraction study to verify the molecular structure of compound **3**. The crystals were obtained by progressive evaporation of the ester solution. The crystal was collected and further analysed leading to unambiguous confirmation of the molecular structure.

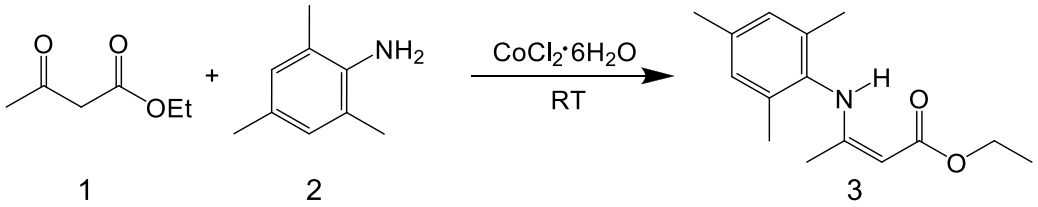

Scheme. 1. **Synthesis of 3-(2,4,6-trimethyl-phenylamino)-but-2-enate.**

The single crystal 3-(2,4,6-trimethyl-phenylamino)-but-2-enoate **3**, picked for X-ray diffraction analysis has the crystal dimensions 0.18×0.12×0.12 mm at 100 K. This compound crystallizes in the monoclinic space group *P*21/c with *Z*= 4, *a*= 8.5003(3) Å, *b*= 20.0682(8) Å, *c*= 8.1720(4) Å, *α*= 90°, *β*= 94.6882(15)°, *γ*= 90°, and *V* = 1389.36 (10) Å³. The crystal structure was determined using 3449 reflections, adhering to the [*F*o>4*σ*(*F*o)] criterion. This resulted in a reliability factor of R= 0.042. Table S1 present all the crystal, collection, and refinement data obtained for this sample at 100(2) K. The ORTEP representation crystal data, conditions of data collection, and the diffraction parameters are illustrated in Figure 1*(a)*.

The aniline C7—N1 (1.4342(15) Å) and the ester C3=O2, C3—O1, O1—C2 bonds length of 1.2254(15) Å, 1.3637(14) Å and 1.4517(15) Å respectively, are typical of the distances observed in aniline and ester compounds [41,42]. The dihedral angle C7—N1—C5—C4, C3—C4—C5—N1, O1—C3—C4—C5 and C2—O1—C3—C4 values of 175.43(12), 0.5 (2), 171.82(12) and −174.07(10)° are closed to 180° revealing that the substituent chain inclosing the enamino ester group is almost linear and deployed in the plane perpendicular to that of the phenyl ring (Figure 1*(a)*). Trimethylamine is almost perpendicular to the *β*-enaminester, forming a dihedral angle of 90°, unlike the same molecule which forms an angle of 88° [40], thanks to that configuration, the H1*N* and O2 atoms are located in the same side allowing intramolecular interaction (Figure 1*(b)*). With H1*N*—O2 distance of 0.855 (17) Å and intramolecular hydrogen bonds can be suggested with a characteristic provided in Table S2. Furthermore, these atoms are implicated in intermolecular interactions as shown in Figure 1*(b)*. The data of these interactions between H1*N* and O2^{i} first, and O2 and H1*N*^{i} secondly, were also reported in Table 2. Finally, when considering a global view of the crystal packing, it appears that hydrogen bond between H1*C* and O2^{ii} with a symmetry code of −x+*2*, −y+*1*, −z+*1* is observed with a bond distance of 2.087 Å (acceptor - donor), this interaction is crucial for understanding the stability of the pseudo-six-membered ring formed between the amide and the ester group [41,42]. The hydrogen bonds and other week molecular interactions stabilizing the crystal packing of this 3-(2,4,6-trimethyl-phenylamino)-but-2-enoate will be described deeply in the next sections. In conclusion, the molecular conformation is stabilized by a strong intramolecular N–H…O, which is in agreement with the ^{1}H NMR analyses.

Hirshfeld surface analysis of compound 3

To gain deeper insights into the molecular interactions present in the crystallographic packing of the described molecule, Hirshfeld surface calculations and interpretations are being explored. The Hirshfeld surfaces and 2D fingerprint plots generated using CrystalExplorer 17.5 are utilized for this purpose [37].

Crystal packing analysis involves investigating the distance from the surface to the nearest nucleus, d_e and d_i (Figure 2*(a)* and *(b)*), to identify probable close interactions. Closed domains appear as red spots on the surface. A more comprehensive description is provided by examining the surface mapped over d_{norm} (Figure 2*(c)*), which is the normalized contact distance, which allows identification of intermolecular interactions on the HS. The HS surface mapped over d_{norm} shows a red spot around the N*H*1 hydrogen atom, confirming the N1—H1N···O2^{i} hydrogen bond. Another red spot is observed around the C=O oxygen atom, confirming the C1—H1C···O2^{ii} intermolecular hydrogen bond. White and blue regions on the surface reveal interactions distances equal and higher than the sum of Van der Waals radii [43,44].

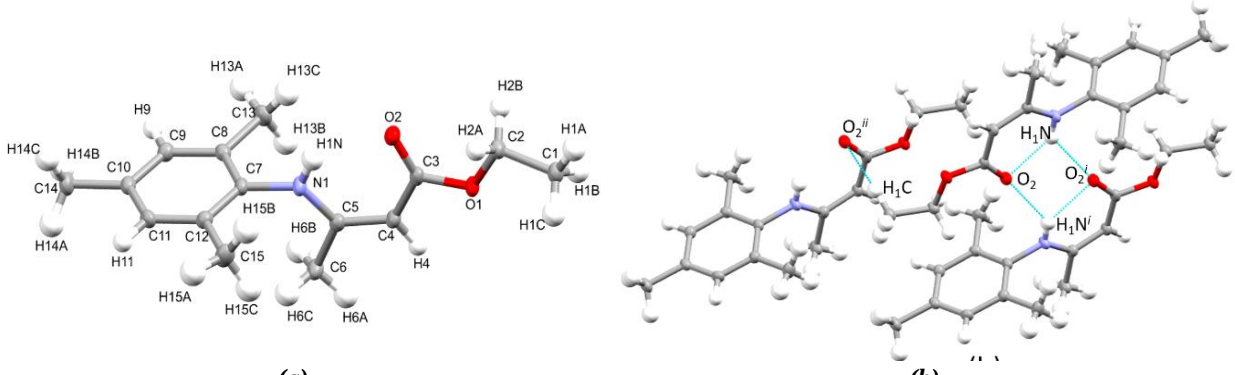

(a) ***(b)***

Figure 1. The molecular structure of compound 3 showing the atom labelling. Displacement ellipsoids are drawn at the 50% probability level (*a*). Representation of intramolecular and intermolecular hydrogen bonds. Symmetry codes: *(i)* −x+*1*, −y+*1*, −z+*1*; (ii) −x+*2*, −y+*1*, −z+*1 (b)*.

The HS mapped over shape-index was then obtained to describe other weak contacts where a molecular surface of the considered molecule touches an adjacent molecular surface. On the HS mapped with shape-index of **3** (Figure 2*(d)*), convex blue regions represent hydrogen donor groups and concave red regions represent acceptor groups [45,46]. There are no regions with adjacent red and blue triangles on the shape-index map indicating a lack of $\pi\cdots\pi$ interactions in the crystal packing. Furthermore, the curvedness property that gives information on "how much shape" is obtained and mapped over the HS in the range of −4 to 4 a.u. [47,48]. Analysis of such surface shows green regions divided by blue boundaries. No large flat green areas on the surface (low values of curvedness) are observed on the surface revealing the absence of π–π planar stacking contact (Figure 2*(e)*). Finally, the electrostatic potentials (EP) for compound **3** were calculated at B3LYP/6-31G(d,p) level of theory [45] and mapped on the Hirshfeld surfaces as shown in Figure 2*(f)*. On the EP surface, the electron-rich and electron-deficient sites in the molecule are represented as blue and red domains corresponding to positive and negative EP respectively. The EP property map reveals that electronegative regions are mainly located around the oxygen atoms. A specific blue spot is observed around the N–H1 atom revealing the electropositive character of that hydrogen atom.

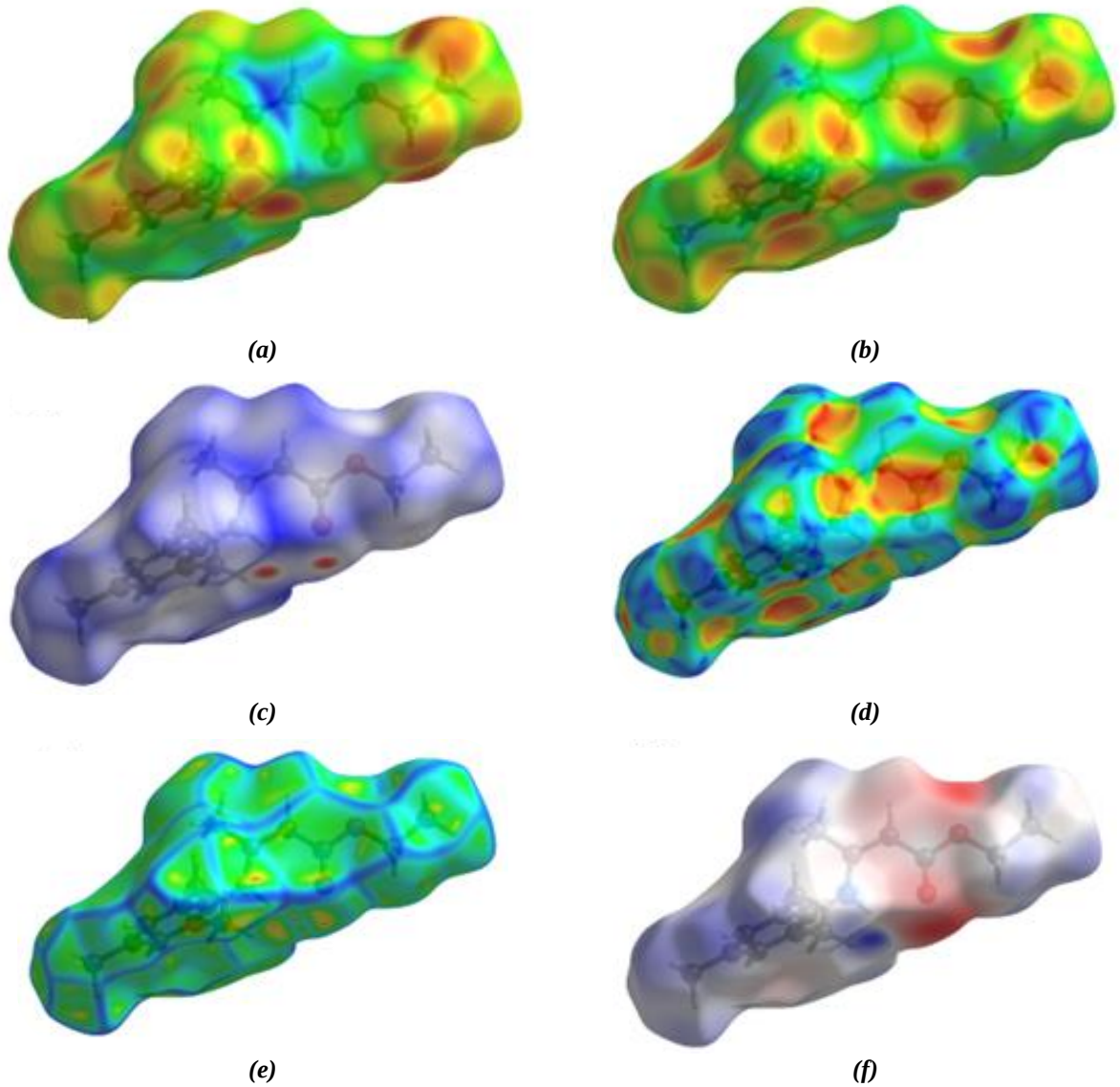

Figure. 2. The Hirshfeld surface of compound 3. Hirshfeld surface mapped with d_i in the range 1.0353 to 2.4839 A *(a)*, d_e in the range 1.0350 to 2.4929 Å *(b)*, d_{norm} in the range -0.1670 to 1.4062 *(c)*, Shape index in the range −1 to 1 *(d)*, Curvedness in the range −4 to 4 *(e)* and ESP in the range −0.0759 to 0.0383 a.u *(f)*.

Molecular fingerprint analysis

The study uses CrystalExplorer 17.5 software to create a molecular fingerprint plot [38], a two-dimensional histogram, to understand intermolecular relationships (Figure 3). The fingerprint, which is decomposed using d_i and d_e, shows that H···H contacts dominate, accounting for 71% of interactions. H···C contacts account for 16%, while O··H interactions at 12.8% confirm hydrogen bonding. Other contacts, such as C···O and N··H, represent only 0.1% each.

Interaction energy and energy framework

The structural description of the ester in this study identifies various intermolecular contacts, whose interaction energies could be assessed and visually represented in energy diagrams. This analysis focuses on a cluster of molecules within a 3.8 Å radius surrounding the selected compound (depicted in black) [49,50]. After the calculation the molecules are colour-coded according to their interaction energy within the cluster. The total intermolecular energy E_{tot} (kJ/mol) relative to the reference molecule (in black) is expressed in terms of four key components: electrostatic, polarization, dispersion, and exchange-repulsion: $E_{tot}= k_{ele} E_{ele} + k_{pol} E_{pol} + k_{dis} E_{dis} + k_{rep} E_{rep}$. The graphical representation of Coulomb interaction energy (red), dispersion energy (green) and total interaction energy (blue) are presented in Figure S4. In this work two approaches have been used to evaluate these energies.

In the first approach using CE-HF electron density level of theory available in CrystalExplorer, the scale factors k_{ele}, k_{pol}, k_{dis} and k_{rep} defined by Spackman and Mackinzie values of 1.019, 0.651, 0.901 and 0.811 must be considered respectively [51]. The values of the total energy components are –53.1 kJ/mol, –18.3 kJ/mol, –222.6 kJ/mol, 112.4 kJ/mol for E_{ele}, E_{pol}, E_{dis} and E_{rep} respectively were obtained after calculation. Altogether, the total interaction energy of –175.3 kJ/mol is obtained. The interaction energy diagram considering this level of theory is present in Figure S4 (left side).

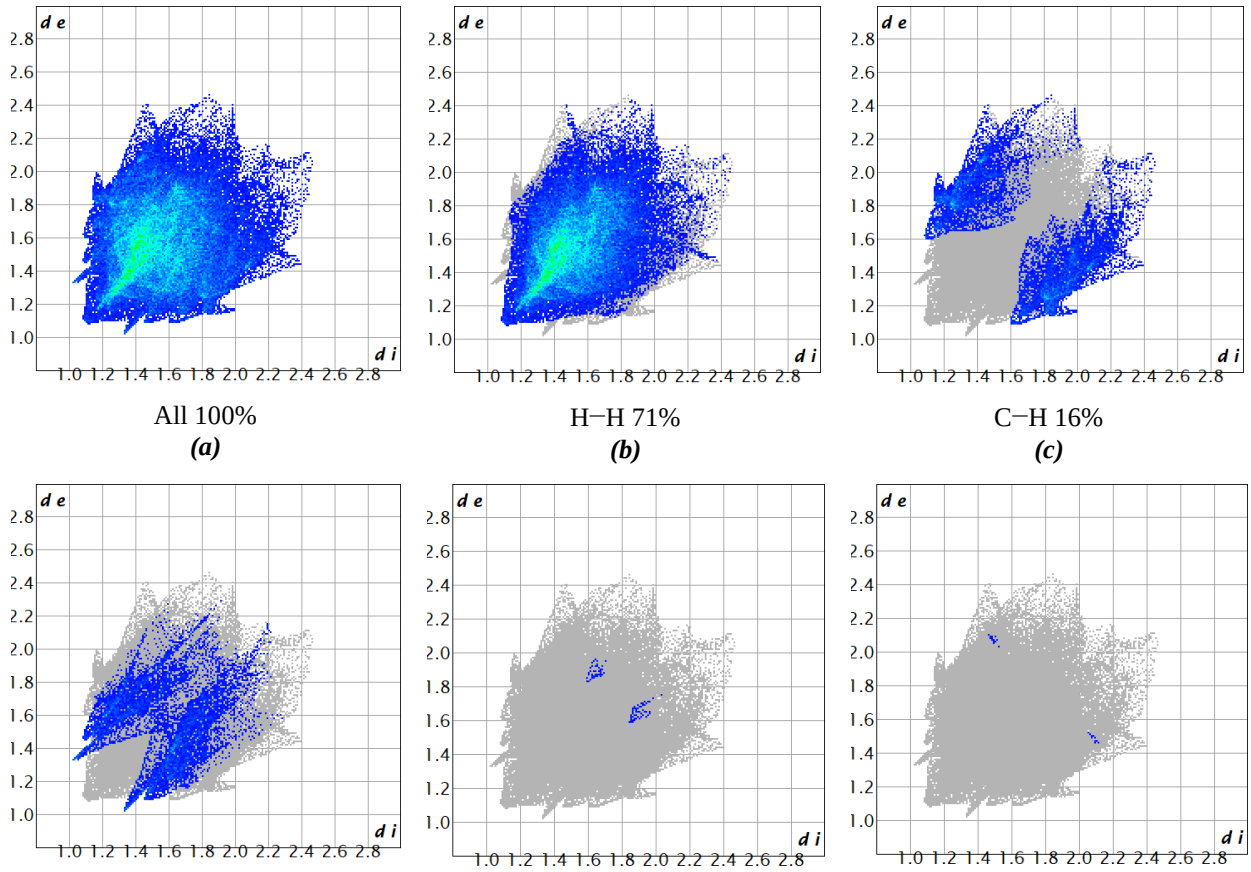

Figure. 3. The two-dimensional fingerprint plots of compound 3 showing all contacts (100%) and decomposed H···H, H···C, H···O, C···O and N···H contacts.

The second approach involved considering the CE-B3LYP/6-31G(d,p) electron density level of theory energy model, which is also available in CrystalExplorer. In that case, the interaction energies components are: E_{ele}= –27.4 kJ/mol, E_{pol}= –12.9 kJ/mol, E_{dis}= –155.7 kJ/mol and E_{rep}= 90.7kJ/mol. For the considered level of theory, the values of the scale factors are k_{ele}= 1.057, k_{pol}= 0.740, k_{dis}= 0.871 and k_{rep} = 0.618 [51]. The calculated total interaction energy obtained is E_{tot} is –118.3 kJ/mol. The energy framework and the different energy components values are resented in Figure S4 (right side). The radii of the cylinders are proportional to the magnitude of interaction energy.

The electrostatic energy framework shows the most significant disparity between the two levels of theory, while dispersion and total interaction energy frameworks show minor differences.

Pharmacokinetic and ADME-Tox prediction

The study analyses the pharmacological potential of *β*-enaminoester, which passes Lipinski's rule of five without violations (Table 1). The molecule's oral bioavailability and toxicity were predicted using the OSIRIS Property Explorer program. Estimations indicate that the molecule is unlikely to exhibit mutagenic, tumorigenic, or irritant properties, indicating its potential for use in various applications.

Good oral bioavailability of a drug is strongly dependent on the balance between hydrophilicity and lipophilicity of the pro-drugs. High hydrophobicity is associated with a high Log*P* value. According to Lipinski's rule of five, a Log*P* value lower than 5.0 and a molecular weight under 500 are indicative of potential oral bioavailability. For the molecule described in this work, with a molecular weight of 247.34 g/mol, a Log*S* of -3.66, and a Log*P* value of 3.72, good oral absorption probability can be expected.

The results indicated a favourable rate of human intestinal absorption at 92.97% [52], implying that it may have an impact on the steady-state volume of distribution in blood plasma [53]. The ADME profile of the compound showed low blood-brain barrier penetration, potential central nervous system safety, and no toxicity with respect to hepatotoxicity and inhibition of hERG I and II channels. However, it may cause skin sensitization.

Conclusion

The synthesis and characterization of novel 3-(2,4,6-trimethyl-phenylamino)-but-2-enoate, as reported in this work, were achieved through a direct condensation reaction in the presence of $CoCl_2$ under solvent-free conditions. Besides using common NMR and IR characterization techniques, X-ray diffraction was employed to confirm the molecular structure of the desired product. The interactions stabilizing the crystal structures were analysed using Hirshfeld surface mapping of various contact descriptors. Additionally, the electron donor and acceptor domains of compound **3** were identified using the shape index and electrostatic potential properties mapped on the Hirshfeld surface. The unique fingerprint plot of the described molecule was presented, and its decomposition revealed that the predominant contacts stabilizing the crystal packing are H···H (71%), C···H (16%), and O···H (12.8%) contacts. This report also presents the first topology of interaction energies stabilizing the structural and packing, considering two levels of theory for the calculation. The results, presented graphically as energy framework diagrams, show a slight discrepancy between the diagram and the values obtained for each model. Finally, in silico pharmacokinetics and physicochemical properties combined with ADME-Tox evaluation indicate that the enaminoester could be considered a drug candidate with predicted non-toxicity.

Table 1

Drug-likeness properties of compound 3 and ADME-Tox prediction.

Property	*Predicted value*	*Property*	*Prediction*
MW	247.34	CYP2D6 substrate	No
Num. rotatable bonds	5	CYP3A4 substrate	No
Num. H-bond acceptor	3	CYP1A2 inhibitor	Yes
Num. H-bond donnors	1	CYP2C19 inhibitor	Yes
Log*P* (*o/w*)	3.72	CYPC2C9 inhibitor	No
Human Intestinal Absorption (%)	92.986	CYP2D6 inhibitor	No
VDss (logL/Kg)	0.251	CYP3A4 inhibitor	No
P-glycoprotein substrate	No	Real OCT2 substrate	No
P-glycoprotein I, II inhibitor	No	AMES toxicity	No
BBB permeability (Log BB)	–0.301	hERG I, II inhibitor	No
CNS permeability (Log PS)	–2.128	Hepatotoxicity	No
Skin Permeability	–2.614	Skin Sensitization	Yes

Acknowledgements

The authors would be thankful for the Bilateral project between CNR Italy and CNRST Morocco (project2020/2021, CUPB54I20000340001, IC-CNR Bari, Italy, A.M., and UMP Oujda, Morocco, R.T.).

Supplementary information

Supplementary data are available free of charge at http://cjm.ichem.md as PDF file.

References

1. Bangalore, P.K.; Vagolu, S.K.; Bollikanda, R.K.; Veeragoni, D.K.; Choudante, P.C.; Misra, S.; Sriram, D.; Sridhar, B.; Kantevari, S. Usnic acid enaminone-coupled 1,2,3-triazoles as antibacterial and antitubercular agents. Journal of Natural Products, 2020, 83(1), pp. 26–35. DOI: https://doi.org/10.1021/acs.jnatprod.9b00475
2. Masocha, W.; Kombian, S.B.; Edafiogho, I.O. Evaluation of the antinociceptive activities of enaminone compounds on the formalin and hot plate tests in mice. Scientific Reports, 2016, 6, 21582, pp. 1–9. DOI: https://doi.org/10.1038/srep21582
3. Amaye, I.J.; Heinbockel, T.; Woods, J.; Wang, Z.; Martin-Caraballo, M.; Jackson-Ayotunde, P. 6 Hz active anticonvulsant fluorinated *N*-benzamide enaminones and their inhibitory neuronal activity. International Journal of Environmental Research and Public Health, 2008, 15(8), 1784, pp. 1–13. DOI: https://doi.org/10.3390/ijerph15081784
4. Cindric, M.; Rubcic, M.; Hrenar, T.; Pisk, J.; Cvijanovic, D.; Lovric, J.; Vrdoljak, V. Novel enaminones as non-cytotoxic compounds with mild antibacterial activity: synthesis and structure-activity correlations. Journal of Molecular Structure, 2018, 1154, pp. 636–642. DOI: https://doi.org/10.1016/j.molstruc.2017.10.078
5. Kumar, L.J.; Sarveswari, S.; Vijayakumar, V. DMFDMA catalyzed synthesis of 2-((Dimethyl amino)methylene)-3,4-dihydro-9-arylacridin-1(2*H*)-ones and their derivatives: *in-vitro* antifungal, antibacterial and antioxidant evaluations. Open Chemistry, 2018, 16(1), pp. 1077–1088. DOI: https://doi.org/10.1515/chem-2018-0110
6. Kumar, R.; Saha, N.; Purohit, P.; Garg, S.K.; Seth, K.; Meena, V.S.; Dubey, S.; Dave, K.; Goyal, R.; Sharma, S.S.; Banerjee, U.C.; Chakraborti, A.K. Cyclic enaminone as new chemotype for selective cyclooxygenase-2 inhibitory, anti-inflammatory, and analgesic activities. European Journal of Medicinal Chemistry, 2019, 182, 111601, pp. 1–15. DOI: https://doi.org/10.1016/j.ejmech.2019.111601
7. Ghorab, M.M.; Ragab, F.A.; Heiba, H.I.; El-Gazzar, M.G.; El-Gazzar, M.G.M. Novel thioureido-benzenesulfonamide derivatives with enaminone linker as potent anticancer, radiosensitizers and VEGFR2 inhibitors. Bioorganic and Medicinal Chemistry Letters, 2018, 28(9), pp. 1464–1470. DOI: https://doi.org/10.1016/j.bmcl.2018.03.089
8. Alexander, M.S.; Scott, K.R.; Harkless, J.; Butcher, R.J.; Jackson-Ayotunde, P.L. Enaminones 11. An examination of some ethyl ester enaminone derivatives as anticonvulsant agents. Bioorganic and Medicinal Chemistry Letters, 2013, 21(11), pp. 3272–3279. DOI: https://doi.org/10.1016/j.bmc.2013.03.036
9. Wang, Z.J.; Sun, L.; Jackson, P.L.; Scott, K.R.; Heinbockel, T. A substituted anilino enaminone acts as a novel positive allosteric modulator of $GABA_A$ receptors in the mouse brain. The Journal of Pharmacology and Experimental Therapeutics, 2011, 336(3), pp. 916–924. DOI: https://doi.org/10.1124/jpet.110.173740
10. Li, Y.; Gao, H.; Zhang, Z.; Qian, P.; Bi, M.; Zha, Z.; Wang, Z. Electrochemical synthesis of *α*-enaminones from aryl ketones. Chemical Communications, 2016, 52(55), pp. 8600–8603. DOI: https://doi.org/10.1039/C6CC03709G
11. Prabakaran, K.; Sivakumar, M.; Perumal, M.S. A simple, efficient green protocol for the synthesis of *β*-enaminone and enamino ester derivatives by using onion extract as green catalyst. ChemistrySelect, 2017, 2(8), pp. 2363–2372. DOI: https://doi.org/10.1002/slct.201601515
12. Harrad, M.A.; Outtouch, R.; Ali, M.A.; El Firdoussi, L.; Karim, A.; Roucoux, A. $Ca(CF_3COO)_2$: An efficient Lewis acid catalyst for chemo- and regio-selective enamination of *β*-dicarbonyl compounds. Catalysis Communications, 2010, 11(5), pp. 442–446. DOI: https://doi.org/10.1016/j.catcom.2009.11.019
13. Rezaei, R.; Shakeri, M. A mild and efficient method for synthesis of *β*-enaminones using melamine-formaldehyde resin supported H^+ under solvent free conditions. Asian Journal of Chemistry, 2013, 25(13), pp.7079–7082. DOI: https://doi.org/10.14233/ajchem.2013.14436
14. Harrad, M.A.; Boualy, B.; El Firdoussi, L.; Ali, M.A. Aluminum phosphate catalyzed free solvent preparation of *β*-enamino esters. American Journal of Chemistry, 2012, 2(5), pp. 271–276. DOI: https://doi.org/10.5923/j.chemistry.20120205.05
15. Harrad, M.A.; Houssini, I.; Boualy, B.; Ouahrouch, A.; Ali, M.A.; Loughzail, M. Natural phosphate as new, highly efficient and reusable heterogeneous catalyst for the selective preparation of *β*-enaminoesters under solvent-free conditions. Chemistry and Materials Research, 2014, 6(3), pp. 31–37. https://www.iiste.org/Journals/index.php/CMR/article/view/11712
16. Eshghi, H.; Seyedi, S.M.; Safaei, E.; Vakili, M.; Farhadipour, A.; Bayat-Mokhtari, M. Silica supported $Fe(HSO_4)_3$ as an efficient, heterogeneous and recyclable catalyst for synthesis of *β*-enaminones and *β*-enamino esters. Journal of Molecular Catalysis A: Chemical, 2012, 363-364, pp. 430–436. DOI: https://doi.org/10.1016/j.molcata.2012.07.021

17. Bhatte, K.D.; Tambade, P.J.; Dhake, K.P.; Bhanage, B.M. Silver nanoparticles as an efficient, heterogeneous and recyclable catalyst for synthesis of *β*-enaminones. Catalysis Communications, 2010, 11(15), pp. 1233–1237. DOI: https://doi.org/10.1016/j.catcom.2010.06.011
18. Feng, C.-L.; Chu, N.-N.; Zhang, S.-G.; Cai, J.; Chen, J.-Q.; Hu, H.-Y.; Ji, M. Solvent-free synthesis of *β*-enamino ketones and esters catalyzed by recyclable iron (III) triflate. Chemical Papers, 2014, 68(8), pp. 1097–1103. DOI: https://doi.org/10.2478/s11696-014-0544-8
19. Gogoi, S.; Bhuyan, R.; Barua, N.C. Iodine-catalyzed conversion of *β*-dicarbonyl compounds into *β*-enaminones within a minute under solvent-free conditions. Synthetic Communications, 2005, 35(21), pp. 2811–2818. DOI: https://doi.org/10.1080/00397910500290557
20. Venkat Narsaiah, A.; Reddy, A.R.; Reddy, B.V.S.; Yadav, J.S. Amberlyst-15®: An efficient, cost-effective and recyclable hetero geneous solid acid catalyst for the synthesis of *β*-enaminones and *β*-enamino esters. The Open Catalysis Journal, 2011, 4, pp. 43–46. DOI: https://doi.org/10.2174/1876214X01104010043
21. Shekhar, A.; Pathak, D.D. Zeolite (ZSM-5) as a highly efficient and heterogeneous catalyst for the synthesis of *β*-enaminones and *β*-enamino esters. Journal of Chemistry. 2011, 8(4), 176829, pp. 1632–1637. DOI: https://doi.org/10.1155/2011/176829
22. Zhang, Z.-H.; Hu, J.-Y. Cobalt (II) chloride-mediated synthesis of beta-enamino compounds under solvent-free conditions. Journal of the Brazilian Chemical Society, 2006, 17(7), pp. 1447–1451. DOI: https://doi.org/10.1590/S0103-50532006000700038
23. Hasaninejad, A.; Zare, A.; Mohammadizadeh, M.R.; Shekouhy, M.; Moosavi-Zare, A.R. A green solventless protocol for the synthesis of *β*-enaminones and *β*-enamino esters using silica sulfuric acid as a highly efficient, heterogeneous and reusable catalyst. Journal of Chemistry, 2010, 7(4), pp. 1546–1554. DOI: https://doi.org/10.1155/2010/829547
24. Harrad, M.A.; Semane, A.; Badereddine, M.; Tounsi, A. $ZnAl_2O_4$@ZnO an effective, heterogeneous catalyst for the synthesis of bis-(*β*-enaminones) and bis-(*β*-enaminoesters). Chemistry Journal of Moldova, 2024, 19(2), pp. 74–82. DOI: https://doi.org/10.19261/cjm.2024.1199
25. Madje, B.R.; Shindalkar, S.S.; Ware, M.N.; Shingare, M.S. An efficient condensation of 4-oxo-4*H*-benzopyran-3-carbaldehydes with 3-methyl-1-phenyl-1*H*-pyrazol-5(4*H*)-one. ARKIVOC, 2005, 14, pp. 82–86. DOI: https://doi.org/10.3998/ark.5550190.0006.e10
26. Etsè, K.S.; Zaragoza, G.; Etsè, K.D. Easy preparation of novel 3,3-dimethyl-3,4-dihydro-2H-1,2,4-benzothiadiazine 1,1-dioxide: molecular structure, Hirshfeld surface, NCI analyses and molecular docking on AMPA receptors. Journal of Molecular Structure, 2021, 1238, 130435, pp. 1–14. DOI: https://doi.org/10.1016/j.molstruc.2021.130435
27. Bruker, APEX II. Bruker AXS Inc., Madison, USA, 2004. https://www.brukersupport.com/ProductDetail/782
28. Sheldrick, G.M. SHELXT–Integrated space-group and crystal-structure determination. Acta Crystallographica A, 2015, A71(1), pp. 3–8. DOI: https://doi.org/10.1107/S2053273314026370
29. Spek, A.L. PLATON SQUEEZE: a tool for the calculation of the disordered solvent contribution to the calculated structure factors. Acta Crystallographica C, 2015, C71, pp. 9–18. DOI: https://doi.org/10.1107/S2053229614024929
30. Farrugia L.J. WinGX and ORTEP for Windows: an update. Journal of Applied Crystallography, 2012, 45, pp. 849–854. DOI: https://doi.org/10.1107/S0021889812029111
31. Macrae, C.F.; Bruno, I.J.; Chisholm, J.A.; Edgington, P.R.; McCabe, P.; Pidcock, E.; Rodriguez-Monge L.; Taylor, R.; Van de Streek, J.; Wood, P.A. Mercury CSD 2.0 – new features for the visualization and investigation of crystal structures. Journal of Applied Crystallography, 2008, 41, pp. 466–470. DOI: https://doi.org/10.1107/S0021889807067908
32. Spackman, P.R.; Yu, L.-J.; Morton, C.J.; Parker, M.W.; Bond, C.S.; Spackman, M.A.; Jayatilaka, D.; Thomas, S.P. Bridging crystal engineering and drug discovery by utilizing intermolecular interactions and molecular shapes in crystals. Angewandte Chemie International Edition, 2019, 58(47), pp. 16780−16784. DOI: https://doi.org/10.1002/anie.201906602
33. McKinnon, J.J.; Spackman, M.A.; Mitchell, A.S. Novel tools for visualizing and exploring intermolecular interactions in molecular crystals. Acta Crystallographica B, 2004, B60, pp. 627−668. DOI: https://doi.org/10.1107/S0108768104020300
34. Etsè, K.D.; Etsè, K.S.; Quashie, M-L.A. Describing auxin solid state intermolecular interactions using contact descriptors, shape property, molecular fingerprint: Comparison of pure auxin crystal and auxin-TIR1 co-crystal. European Journal of Chemistry, 2022, 13(2), pp. 172–179. DOI: https://doi.org/10.5155/eurjchem.13.2.172-179.2271
35. Hunter, C.A.; Singh, J.; Thornton, J.M. *π*-*π* interactions: the geometry and energetics of phenylalanine-phenylalanine interactions in proteins. Journal of Molecular Biology, 1991, 218(4), pp. 837−846. DOI: https://doi.org/10.1016/0022-2836(91)90271-7
36. Singh, J.; Thornton, J.M. SIRIUS: An automated method for the analysis of the preferred packing arrangements between protein groups. Journal of Molecular Biology, 1990, 211(3), pp. 595−615. DOI: https://doi.org/10.1016/0022-2836(90)90268-Q

37. CrystalExplorer17. University of Western Australia, 2017. https://crystalexplorer.net/
38. Spackman, M.A.; McKinnon, J.J. Fingerprinting intermolecular interactions in molecular crystals. CrystEngComm, 2002, 4(66), pp. 378–392. DOI: https://doi.org/10.1039/b203191b
39. Pérez-Bonilla, M.; Castro, J.M.; Linares-Palomino, P.J.; Altarejos, J.; Nogueras, M.; Sánchez, A.; Salido, S. (*Z*)-2-Methyl-3-(1-phenyl-ethyl amino)-but-2enoic acid ethyl ester. Molbank, 2005, 2005(1), M395. DOI: https://doi.org/10.3390/M395
40. Amézquita-Valencia, M.; Hernández-Ortega; S.; Suárez-Ortiz, G.A.; Toscano, R.A.; Cabrera, A. (*Z*)-Ethyl 3-(2,4,6-trimethylanilino)but-2-enoate. Acta Crystallographica E, 2009, 65(11), pp. o2728. DOI: https://doi.org/10.1107/S160053680903949X
41. Atlas, S.; Etsè, K.S.; Guillermo, Z.V.; Maatallah, M.; Tounsi, A.; Harrad, M.A. Structural and quantum study of newly synthesized methyl(*Z*)-3-((4-fluorophenyl) amino) but-2-enoate. Advanced Journal of Chemistry A, 2025, 8(4), pp. 809–824. DOI: https://doi.org/10.48309/AJCA.2025.471262.1623
42. Nossa González, D.L.; Saeed, A.; Shabir, G.; Flörke, U.; Erben, M.F. Conformational and crystal structure of acyl thiourea compounds: The case of the simple (2,2-dimethyl-propionyl) thiourea derivative. Journal of Molecular Structure, 2020, 1215, 128227, pp. 1–8. DOI: https://doi.org/10.1016/j.molstruc.2020.128227
43. Etsè, K.S.; Dassonneville, B.; Zaragoza, G.; Demonceau, A. One-pot, Pd/Cu-catalysed synthesis of alkynyl-substituted 3-ylidene-dihydrobenzo[d]isothiazole 1,1-dioxides. Tetrahedron Letters, 2017, 58(8), pp. 789–793. DOI: https://doi.org/10.1016/j.tetlet.2017.01.041
44. Etsè, K.S.; Zaragoza, G.; Pirotte, B. Crystal structure and Hirshfeld surface analysis of *N*-(2-(N-methylsulfamoyl)-phenyl)-formamide: degradation product of 2-methyl-2*H*-1,2,4-benzothiadiazine 1,1-dioxide. European Journal of Chemistry, 2019, 10(3), pp. 189–194. DOI: https://doi.org/10.5155/eurjchem.10.3.189-194.1903
45. Etsè, K.S.; Zaragoza, G.; Etsè, K.D. Easy preparation of novel 3,3-dimethyl-3,4-dihydro-2*H*-1,2,4-benzothiadiazine 1,1-dioxide: molecular structure, Hirshfeld surface, NCI analyses and molecular docking on AMPA receptors. Journal of Molecular Structure, 2021, 1238, pp. 130435. DOI: https://doi.org/10.1016/j.molstruc.2021.130435
46. Spackman, M.A.; Jayatilaka, D. Hirshfeld surface analysis. CrystEngComm, 2009, 11(1), pp. 19–32. DOI: https://doi.org/10.1039/B818330A
47. Etsè, K.S.; Zaragoza, G. Insight into structural description of novel 1,4-Diacetyl-3,6-bis(phenylmethyl)-2,5-piperazinedione: synthesis, NMR, IR, Raman, X-ray, Hirshfeld surface, DFT and docking on breast cancer resistance protein. Journal of Molecular Structure, 2022, 1248, pp. 131435. DOI: https://doi.org/10.1016/j.molstruc.2021.131435
48. Spackman, M.A.; McKinnon, J.J.; Jayatilaka, D. Electrostatic potentials mapped on Hirshfeld surfaces provide direct insight into intermolecular interactions in crystals. CrystEngComm, 2008, 10(4), pp. 377−388. DOI: https://doi.org/10.1039/B715227B
49. Boukhssas, S.; Aouine, Y.; Faraj, H.; Alami, A.; El Hallaoui, A.; Tijani, N.; Yamni, K.; Zouihri, H.; Mrani, D.; Lachkar, M. Hirshfeld surface analysis and DFT calculations of 1-phenyl-*N*(benzomethyl)-*N*-({1-[(2-benzo-4-methyl-4,5-dihydro-1,3-oxazol-4yl)-methyl]-1*H*-1,2,3-triazol-4-yl}-methyl)-methanamine. Journal of Materials and Environmental Sciences, 2018, 9(8), pp. 2254−2262. https://www.jmaterenvironsci.com/
50. Etsè, K.S.; Zaragoza, G.; Boschini, F.; Mahmoud, A. New *N*-methylimidazolium hexachloroantimonate: synthesis, crystal structure, Hirshfeld surface and catalytic activity of in cyclopropanation of stryrene. Inorganic Chemistry Communications, 2020, 122, pp. 108291. DOI: https://doi.org/10.1016/j.inoche.2020.108291
51. Turner, M.J.; Thomas, S.P.; Shi, M.W.; Jayatilaka, D.; Spackman, M.A. Energy frameworks: insights into interaction anisotropy and the mechanical properties of molecular crystals. Chemical Communications, 2015, 51(18), pp. 3735–3738. DOI: https://doi.org/10.1039/C4CC09074H
52. Yan, A.; Wang, Z.; Cai, Z. Prediction of human intestinal absorption by GA feature selection and support vector machine regression. International Journal of Molecular Sciences, 2008, 9(10), pp. 1961–1976. DOI: https://doi.org/10.3390/ijms9101961
53. Pires, D.E.V.; Ascher, D.B.; Blundell, T.L. mCSM: predicting the effects of mutations in proteins using graph-based signatures. Bioinformatics, 2014, 30(3), pp. 335–342. DOI: https://doi.org/10.1093/bioinformatics/btt691